Supporting Information (SI)

Interaction between Surface-charge Modified Gold Nanoparticles and Phospholipid Membranes †

Xueqing Xing [a‡], Wanshun Ma [b‡], Xiaoyi Zhao [ac], Jiayi Wang [ac], Lei Yao [a], Xingyu Jiang [b*], Zhonghua Wu [ac*]

[a] *Beijing Synchrotron Radiation Facility, Institute of High Energy Physics, Chinese Academy of Sciences, Beijing 100049, China, E-mail: wuzh@ihep.ac.cn*

[b] *CAS Key Lab for Biological Effects of Nanomaterials and Nanosafety, National Center for NanoScience and Technology, Beijing 100190, China. E-mail: xingyujiang@nanoctr.cn*

[c] *University of Chinese Academy of Sciences, Beijing 100049, China.*

‡: *Xueqing Xing and Wanshun Ma contributed equally to this study.*

Contents

SI-1. Materials

Sample preparation of gold nanoparticles.

The gold nanoparticles (AuNPs) without surface modification were prepared through the seeding growth approach and the average particle size of is about 6.0 nm in diameter. The standard deviation of the particle sizes is about 10%. Therefore, these as-prepared AuNPs are relatively uniform. In order to get different surface charges, the as-prepared AuNPs were, respectively, surface-modified with the following four molecules: $HS(CH_2)_{11}SO_3Na$, $HS(CH_2)_{10}COOH$, $HS(CH_2)_{11}NH_3Cl$, and $HS(CH_2)_{11}N(CH_3)_3Cl$. The four small molecules have the same carbon-chain lengths but different end-groups. $SH(CH_2)_{11}SO_3Na$ molecule provides the one-valence negative ligand [$-S(CH_2)_{10}-SO_3^-$] bonded to the surface of AuNPs. $SH(CH_2)_{10}COOH$ molecule provides another one-valence negative ligand [$-S(CH_2)_{10}COO^-$] bonded to the surface of AuNPs. $SH(CH_2)_{11}NH_3Cl$ molecule provides the one-valence positive ligand [$-S(CH_2)_{10}-NH_3^+$] bonded to the surface of AuNPs. And $HS(CH_2)_{11}N(CH_3)_3Cl$ molecule provides another one-valence positive ligand [$-S(CH_2)_{11}N(CH_3)_3^+$] bonded to the surface of AuNPs. After the surface modification, the four modified AuNPs are, respectively, marked as $AuSO_3^-$, $AuCOO^-$, $AuNH_3^+$ and $AuNMe_3^+$. Besides the four kinds of surface-modified AuNPs, the as-prepared AuNPs can be used as neutral AuNPs and marked as Au^0. Therefore, there are altogether five kinds of available AuNPs in this study.

Sample preparation of mimicked cell membranes for SAXS observation.

Three kinds of phospholipid molecules were used to compose mimicked membranes. All these phospholipids used in experiments were purchased from Avanti Polar Lipids and used without further purification. Three lipid membranes composed of DOPC, DOPG, and DOPE were prepared. They are, respectively, the PC membrane which consists of 100% DOPC, the PCPG membrane which consists of DOPC and DOPG molecules with a mole ratio of DOPC:DOPG=4:1, and the PEPG membrane which consists of DOPE and DOPG molecules with a mole ratio of DOPE:DOPG=4:1. The PC membrane was used to mimic the eukaryotic cell membrane. The PEPG membrane was used to mimic prokaryotic cell membrane. And the PCPG membrane was used as a control. Three small unilamellar vesicles of PC, PCPG, and PEPG were prepared by following the preparation method [a] recommended by the Avanti Company. The suspensions of the three unilamellar vesicles were all 16

mg/ml. The as-prepared three unilamellar vesicles all have uniform sizes of about 200 nm in diameter.

Sample preparation of giant unilamellar vesicles for Laser confocal fluorescence microscopy observation.

In order to judge whether the PEPG membranes were destroyed or whether some pore structures were formed on the membranes after treatment with positive charged $AuNH_3^+$ AuNPs, laser confocal fluorescence microscope (CFM) was used to observe the possible leakage and structure changes of the lipid membranes. For this sake, giant unilamellar vesicles (GUV) of the mimic membranes were prepared using the Electroformation-ITO Glass method. The obtained GUV size is in micron level. In the preparation of GUV, a layer (~1 nm) of red dyed molecules (DiI) with emission wavelength of 565 nm was inserted into the membrane of the GUVs, which is used to characterize the presence of the GUVs in the suspensions. A sucrose solution with a concentration of 200 mM was also prepared in which the dyed molecules calcein with emission wavelength of 517 nm was dissolved. These dyed molecules make the sucrose solution to show yellow as observed by naked eyes or green under green light of CFM. Then, the suspension of PEPG GUVs was mixed with the sucrose solution. The mixture suspension was observed under red light with excitation wavelength of 549 nm or green light with excitation wavelength of 494 nm. By the color change of the GUVs before and after adding AuNPs to the mixture solution, the possible infiltration of the mixture suspension into the GUVs can be determined.

SI-2. Methods

SAXS Measurements and data analysis.

For comparing the effects of the five AuNPs on the three mimic membranes, each of the five AuNPs were, respectively, added into the three suspensions of the mimic membranes to get the mixture suspensions. Then these mixture suspensions and the pure suspensions of the three mimic membranes were used for SAXS measurements. These SAXS experiments were performed at Beamline 1W2A of the Beijing Synchrotron Radiation Facility (BSRF). The incident X-ray beam was monochromized to a wavelength (λ) of 1.54 Å by a Si(111) triangle bending crystal. A Mar165 two-dimensional charge coupled device (CCD) detector with 2048 × 2048

pixels (each pixel size is 79×79 μm^2) was used to record the SAXS patterns. The sample-to-detector distance was fixed at 1485 mm, covering a q-range of 0.32-3.14 nm^{-1}. Here, $q=4\pi\cdot\sin\theta/\lambda$, is the scattering vector and 2θ is the scattering angle. During the SAXS measurements, the aqueous samples were injected into a tailor-made sample holder. All sample thicknesses in X-ray path were controlled to be 1 mm for best signal-to-noise ratios. In order to compare conveniently the changes of SAXS signals, all the collected two-dimensional SAXS patterns were firstly transformed to one-dimensional SAXS curves by using the Fit2d program [b] then the SAXS intensities were normalized to the direct beam intensities and the buffer scattering were removed.

PEPG vesicle leakage assay.

The CFM observations were used for PEPG vesicle leakage assay shown in Fig. S4. The sucrose solution of the PEPG GUVs without the $AuNH_3^+$ nanoparticles was first observed under green light (Fig. S2A). It can be found that the background is green because of the calcein molecules dissolved in the sucrose solution. While the PEPG GUVs display as black discs because the calcein cannot enter the interior of the intact PEPG GUVs. Then, the sucrose solution of the PEPG GUVs with the $AuNH_3^+$ nanoparticles was also observed under green light and the corresponding CFM is shown in Fig. S4. It can be found that the background is still green because of the calcein dissolved in the sucrose solution. But the PEPG GUVs are invisible because the leakage of PEPG GUVs occurred and the calcein has easily entered the interior of the PEPG GUVs through the transmembrane pores. This result confirms that the positive-charged $AuNH_3^+$ nanoparticles indeed induce the formation of the transmembrane pores or water channels on the PEPG membranes.

Electron density calculation.

The electron density $\rho(x, y)$ of the centrosymmetrical two-dimensional (2D) hexagonal structure can be expressed as Eq. (S1) with the Fourier synthesis technique.

$$\rho_{\mathrm{hex}}(x,y) = \rho_{\mathrm{avg}} + \sum_{\mathrm{h}=1}^{\infty}\sum_{\mathrm{k}=1}^{\infty} A_{\mathrm{hk}}\big[\cos(\mathrm{hB}+\mathrm{kC}) + \cos(\mathrm{hB}-(\mathrm{h}+\mathrm{k})C) + \cos\big((\mathrm{h}+\mathrm{k})B-\mathrm{kC}\big)\big] + \sum_{\mathrm{h}=0}^{\infty}\sum_{\mathrm{k}=0}^{\infty} A_{\mathrm{hk}}^{(\mathrm{h}\neq 0 \text{ and } \mathrm{k}=0) \text{ or } (\mathrm{h}=0 \text{ and } \mathrm{k}\neq 0)}[\cos(\mathrm{hB}+\mathrm{kC}) + \cos((\mathrm{h}+\mathrm{k})(B-\mathrm{C}))/2]. \quad (S1)$$

Where,

$$\mathrm{B} = \frac{2\pi(x+y\cot(\pi/3))}{d},$$

$$\mathrm{C} = \frac{2\pi y}{d\sin(\pi/3)}.$$

Here, x and y are defined as two mutual orthogonal directions. It is known that $I_{\mathrm{hk}} \propto mA_{\mathrm{hk}}^2/\sin\theta$, I_{hk} is the integrated intensity of the (hk) diffraction peak, $\sin\theta$ is the Lorentz factor, and m is the multiplicity factor. Therefore, the scattering amplitude A_{hk} can be extracted from the diffraction patterns. In the electron-density calculation, m=6 for the (10), (11), (20), and (30) reflections, and m=12 for the (21) reflection. Gaussian function was used to fit the five peak profiles and get their integrated intensities I_{hk}. The scattering-amplitude ratios of the five peaks were obtained to be 1.000: 0.790: 0.537: 0.107: 0.116. However, the scattering phases cannot be extracted from the five peaks. Fortunately, the phases of the five peaks can be chosen as (+, -, -, +, +) according to the Turner and Gruner's swelling method.

SI-3. Supporting figures

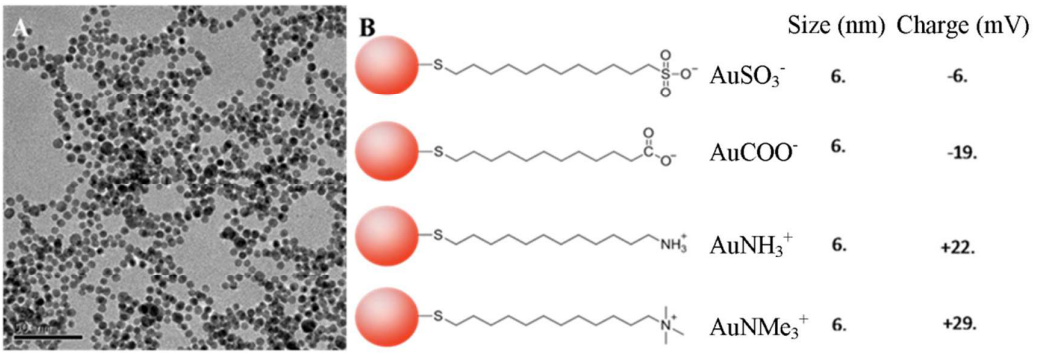

Figure S1. (A). TEM result of the synthesized non coated AuNPs (marked as Au^0). (B). Sketch maps of surface-modified AuNPs with, respectively, $HS(CH_2)_{11}SO_3Na$, $HS(CH_2)_{10}COOH$, $HS(CH_2)_{11}NH_3Cl$, and $HS(CH_2)_{11}N(CH_3)_3Cl$, (marked as $AuSO_3^-$, $AuCOO^-$, $AuNH_3^+$, and $AuNMe_3^+$). The diameter of the non coated AuNPs is 6 nm and the effective potentials of the four surface-modified AuNPs are also shown here.

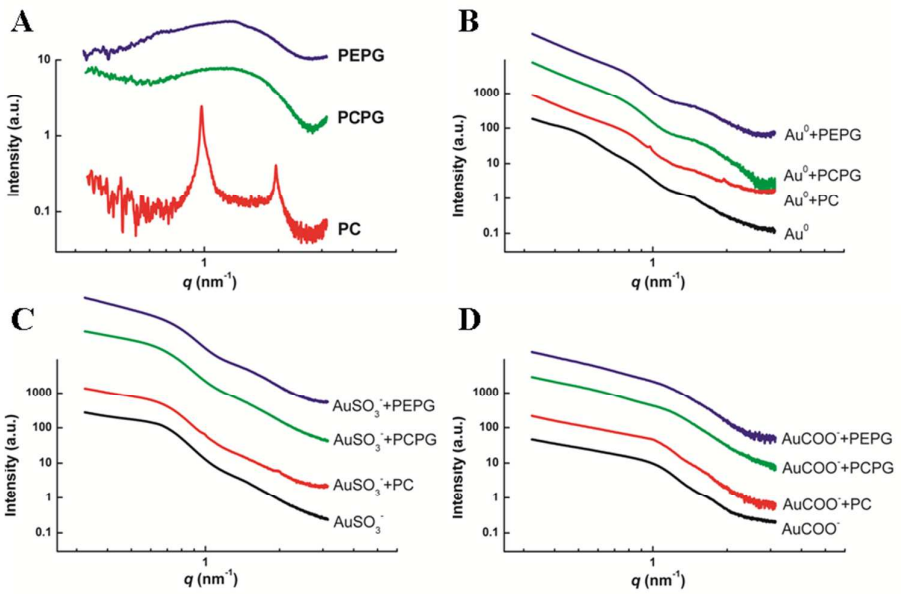

Figure S2. (A). SAXS-curve comparison of three mimic-membrane suspensions (PC, PCPG, and PEPG). (B). SAXS-curve comparison of non coated Au^0 nanoparticle suspension and the three mixture suspensions of Au^0 and the mimic membranes (Au^0+PC, Au^0+PCPG, Au^0+PEPG). (C). SAXS-curve comparison of $AuSO_3^-$ nanoparticle suspension and the three mixture suspensions of $AuSO_3^-$ and the mimic membranes ($AuSO_3^-$+PC, $AuSO_3^-$+PCPG, $AuSO_3^-$+PEPG). (D). SAXS-curve comparison of $AuCOO^-$ nanoparticle suspension and the three mixture suspensions of $AuCOO^-$ and the mimic membranes ($AuCOO^-$+PC, $AuCOO^-$+PCPG, $AuCOO^-$+PEPG).

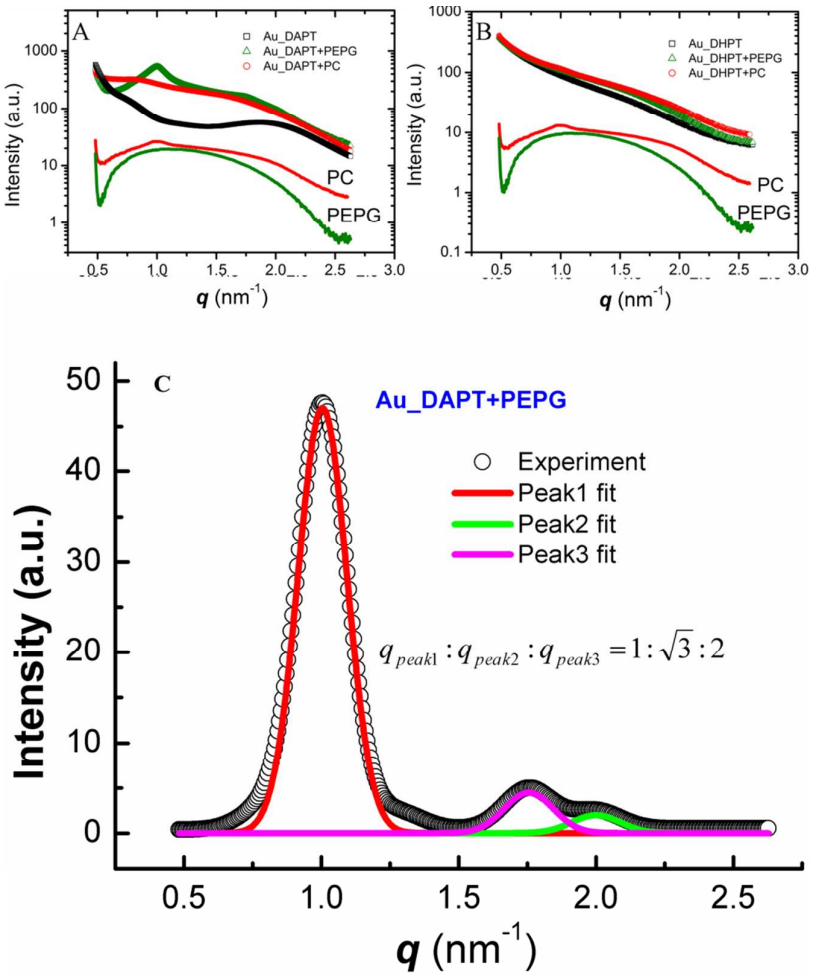

Figure S3. (A). SAXS-curve comparison of PC and PEPG membrane, Au_DAPT, and mixture suspesions of Au_DAPT+PEPG and Au_DAPT+PC. (B). SAXS-curve comparison of PC and PEPG membrane, Au_DHPT, and mixture suspesions of Au_DHPT+PEPG and Au_DHPT+PC. (C). The SAXS-curve of Au_DAPT+PEPG with the scattering background subtracted, and the three diffraction peaks were prominent and fitted by Peakfit program. The ratio of the three peak positions is $1:\sqrt{3}:2$, indicating that the PEPG membranes have been transformed into H_{II} phase by Au_DAPT nanoparticles.

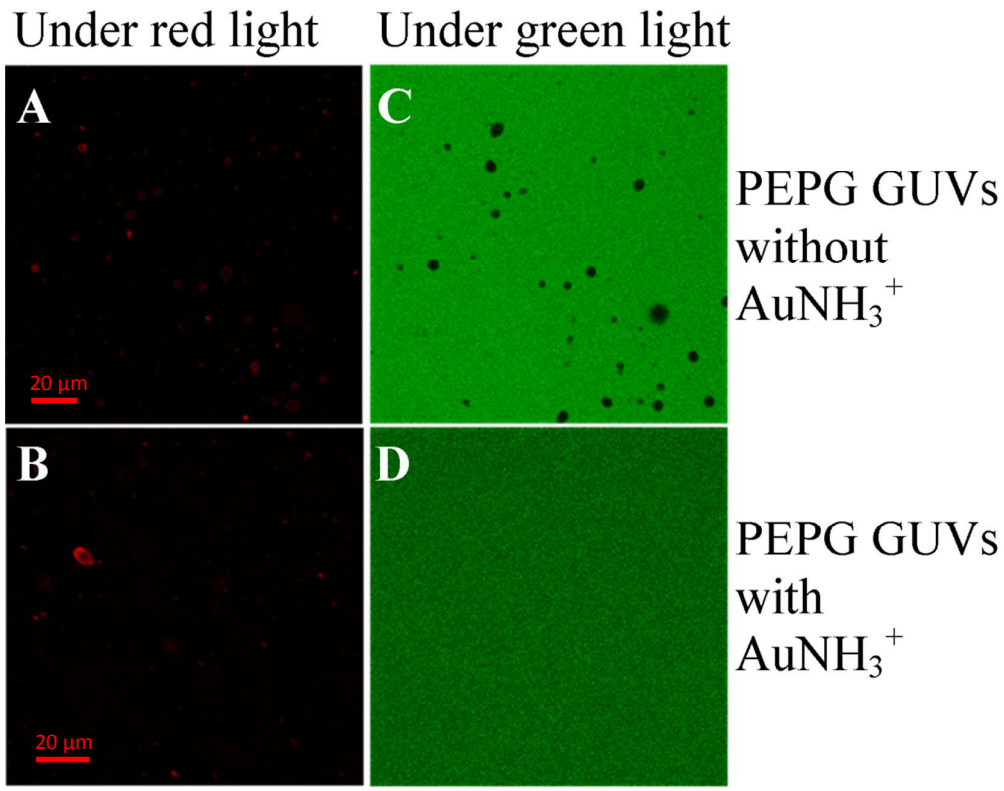

Figure S4. Confocal fluorescence micrographs of PEPG GUVs sucrose solution with or without the presence of $AuNH_3^+$ nanoparticles. (A). PEPG GUVs without the presence of $AuNH_3^+$ nanoparticles display as red circles in black background as the red dyed molecules (DiI) was inserted into the PEPG membrane, which demonstrates that PEPG indeed forms vesicles in the sucrose solution. (B). PEPG GUVs with the presence of $AuNH_3^+$ nanoparticles still display as red circles in back background because the red dyed molecules (DiI) was only inserted into the PEPG membrane even though the leakage of PEPG vesicles occurred. The suspension was observed under red light for (A) and (B). (C). PEPG GUVs without the presence of $AuNH_3^+$ nanoparticles display as black discs in green background as the calcein dyed molecules were only dissolved in the sucrose solution, not in the interior of GUVs. That means the PEPG GUVs maintains intact status before the $AuNH_3^+$ nanoparticles were added. (D). PEPG GUVs with the presence of $AuNH_3^+$ nanoparticles is invisible in green background because the leakage of PEPG GUVs occurred and the calcein dyed molecules entered the interior of PEPG GUVs. The suspension was under green light for (C) and (D). The scale bar is 20µm.

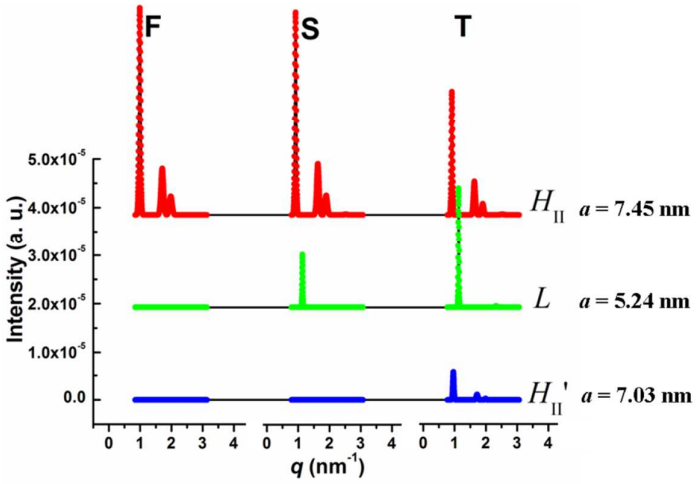

Figure S5. Evolution of phase contents and lattice parameters of the PEPG+$AuNMe_3^+$ sample. At the first 10 minutes, an inverted hexagonal phase (named as H_{II}) with lattice parameter of 7.45 nm was formed. At the second 10 minutes, the H_{II} phase slightly lowered, and a new lamellar phase (L) with lattice parameter of 5.24 nm was forming. At the third 10 minutes, the content of H_{II} phase greatly lowered and the content of L phase fast increased, at the same time a new inverted hexagonal phase (named as H_{II}') with lattice parameter of 7.03 nm was forming.

SI-4. Electrostatic interaction

In order to evaluate the electrostatic interaction between the lipid vesicle (or micelle) and the positively-charged AuNPs, two kind brief models (Fig. S6(a), micelle model; and Fig. S6(b), vesicle model) were adopted. In both models, the outer positive charges from the headgroups of PE or PC are assumed to distribute uniformly on a spherical surface with radius of R, while the outer negative charges from the headgroups of PE or PC and PG are assumed to distribute uniformly on a spherical surface with radius of R-δ. Here δ is the distance between the negative and positive charges in the headgroups. In the vesicle model, the inner negative and positive charges are assumed to distribute uniformly on the spherical surfaces with radius of R-δ-λ and R-2δ-λ, respectively. Here the distance between two negative-charge layers is defined as λ. The positively-charged AuNP locate at position A, which is r far away from the center O of the lipid micelle or vesicle. Then we define: $r=xR$, $\delta=yR$, $\delta+\lambda=zR$, and $2\delta+\lambda=wR$.

We assume that the number of lipid molecules (PC, or PE, and PG) in a micelle or vesicle is N. then the total number of negative charges is N in one negative-charge layer, but the number of positive charges is $4N/5$ in one positive-charge layer. Based on the models, the charge densities (q) on the spherical surfaces can be easily expressed. We assume that the AuNP has $+Q$ charge, then the electrostatic repulsion between the outer positive-charge layer (the first layer) in the micelle or vesicle and the AuNP can be expressed as follow.

$$F_1 = k\frac{\int_0^{\pi} Qqds}{r^2} = kQ\frac{\int_0^{\pi} \frac{4Ne}{5}\cdot\frac{1}{4\pi R^2}\cdot 2\pi R\sin\theta_1\cdot Rd\theta_1\cdot\cos\alpha_1}{r'^2}. \qquad (S2)$$

Where,

$$\cos\alpha_1 = \frac{r - R\cos\theta}{r'},$$

$$r'^2 = R^2 + r^2 - 2rR\cos\theta, \qquad (S3)$$

$$r = xR.$$

Replace Eq. (S3) into Eq. (S2), then we can obtain:

$$F_1 = \frac{2kNeQ}{5R^2}\int_0^{\pi} \frac{(x-\cos\theta)\sin\theta}{\left[1+x^2-2x\cos\theta\right]^{3/2}}d\theta. \qquad (S4)$$

In the same way, we can obtain the electrostatic repulsions between the second (negative charge), the third (negative charge), and the fourth (positive charge) layers and the AuNP as follows.

$$F_2 = -\frac{kNeQ}{2R^2}\int_0^{\pi} \frac{(1-y)^2[x-(1-y)\cos\theta]\sin\theta}{\left[(1-y)^2+x^2-2x(1-y)\cos\theta\right]^{3/2}}d\theta, \qquad (S5)$$

$$F_3 = -\frac{kNeQ}{2R^2}\int_0^{\pi} \frac{(1-z)^2[x-(1-z)\cos\theta]\sin\theta}{\left[(1-z)^2+x^2-2x(1-z)\cos\theta\right]^{3/2}}d\theta, \qquad (S6)$$

$$F_4 = \frac{2kNeQ}{5R^2}\int_0^{\pi} \frac{(1-w)^2[x-(1-w)\cos\theta]\sin\theta}{\left[(1-w)^2+x^2-2x(1-w)\cos\theta\right]^{3/2}}d\theta. \qquad (S7)$$

The total electrostatic repulsion $F=F_1+F_2+F_3+F_4$. When only F1 and F2 are kept, it is the case of micelle model. When all F_1, F_2, F_3, and F_4 are kept, it is the vesicle model.

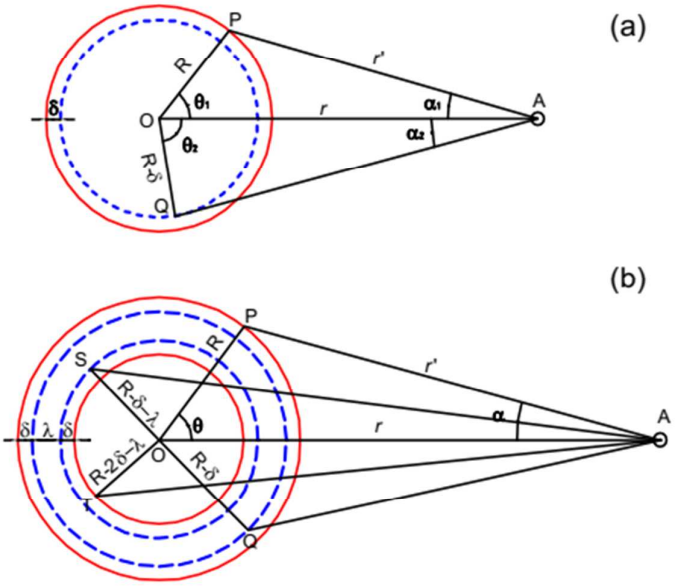

Figure S6. Models of electrostatic interactions between lipid micelle (a) or lipid vesicle (b) and positively-charged AuNP.

The total electrostatic repulsion has been calculated based on Eqs. (*S*4), (*S*5), (*S*6), and (*S*7). As we take δ=0 (i.e. y=0), it is the single electric-layer models. Otherwise, it is the double electric-layer models. In the numerical calculations, four sets of parameters are used as listed in Fig. S7, which are corresponding to the double electric-layer micelle model (y=0.005), single electric-layer micelle model (y=0), double electric-layer vesicle model (y=0.005, z=0.055, w=0.06), and single electric-layer vesicle model (y=0, z=0.052, w=0.52), respectively. The calculated electrostatic repulsions are shown in Fig. S7. It can be found that the electrostatic attraction (negative values) always reaches its maximum when the AuNP moves onto the surface (i.e. *r*=*R*) of the lipid micelle or the lipid vesicle.

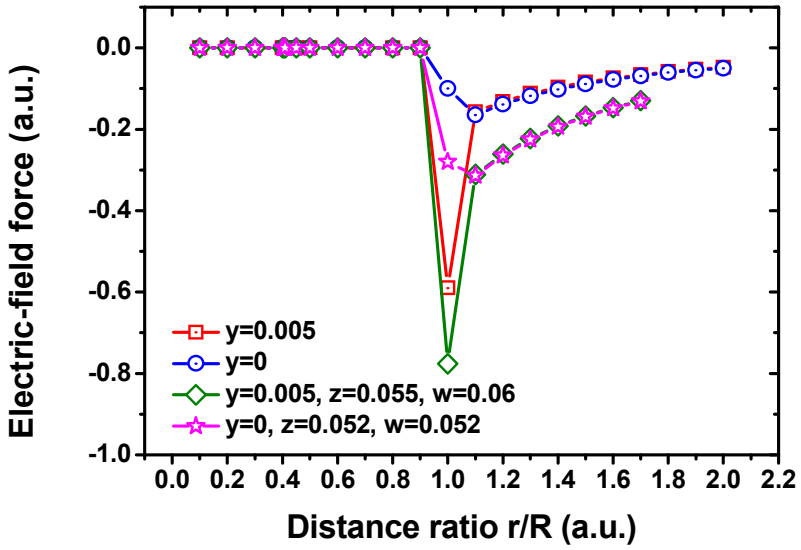

Figure S7. Numerical modelings of the electrostatic interactions between lipid micelle or vesicle and positively-charged AuNP.

References:

(a) website:
http://www.avantilipids.com/index.php?option=com-content&view=article&id=1384&Itemid=372
(b) ESRF website: http://www.esrf.eu/computing/scientific/FIT2D/